Received May 1, 2020, accepted May 6, 2020, date of publication May 11, 2020, date of current version June 4, 2020.

Digital Object Identifier 10.1109/ACCESS.2020.2993707

A Narrow Groove Structure Based Plasmonic Refractive Index Sensor

YANJUN HU, YULONG HOU, ABDUL GHAFFAR, AND WENYI LIU
Science and Technology on Electronic Test and Measurement Laboratory, North University of China, Taiyuan 030051, China

Corresponding author: Wenyi Liu (liuwenyi@nuc.edu.cn)

This work was supported in part by the Fund for Shanxi 1331 Project Key Subject Construction, and in part by the National Science Foundation of Shanxi Province, China, under Grant 201701D121065.

ABSTRACT A refractive index (RI) sensor based on plastic optical fiber (POF) with narrow groove structures coated with a gold layer (POF-NGS (Au)) is proposed and demonstrated. The proposed sensor was characterized using intensity interrogation, where the change in transmission power is induced by light filed interaction and Surface Plasmon Resonance (SPR). Narrow groove structures with lengths of 5 mm were fabricated using an ultraviolet laser, and a gold layer was sputtered to the surface of the whole fiber. The effect of the machining pitch on the RI response was studied. In this paper, dB and μW were used to represent the change of transmission power. Experiments have shown that the POF-NGS (Au) RI sensor has liner response between 1.340 and 1.356. The curvature of the output is largest when the machining pitch is 400 μm with sensitivity 12.5 dB/RIU (126 μW/RIU). The repeatability and temperature sensitivity characteristics were also characterized. Furthermore, the proposed sensor offers improved stability and signal to noise ratio.

INDEX TERMS Narrow groove structures (NGS), intensity interrogation, light filed interaction, surface Plasmon resonance (SPR).

I. INTRODUCTION

Different types of optical fiber refractive index (RI) sensors have been reported. Fiber-Grating [1]–[6], Michelson interferometer and Febry–Perot [7]–[9] based on glass optical fibers (GOFs) have been extensively studied. However, the Fiber-Grating sensors are cross-sensitive to temperature and strain, which affects measurement accuracy. Michelson and Febry–Perot interferometer sensors have the disadvantages of difficulty in processing and system construction. Photonic crystal fibers (PCFs) can change its light propagation mode by changing parameters such as the arrangement and size of pores in the cladding area. Nevertheless, PCFs are expensive and many sensors are still in simulation and theoretical analysis [10]–[12]. Compared with the above sensors based on GOFs, plastic optical fibers (POFs) have the advantages of low-cost, flexible, large diameter, and easy processing. In terms of interrogation method, wavelength interrogation is widely used in GOFs and PCFs sensors, but it requires expensive experimental equipment. In this paper, the use of intensity interrogation for POFs sensors provides a possibility for low-cost and simple experimental systems.

The associate editor coordinating the review of this manuscript and approving it for publication was Zinan Wang.

Surface Plasmon Resonance (SPR) occurs at the interface between a prism and an adjacent metal layer, which is a useful effect in optical fiber RI detection. Compared to prism SPR sensors, SPR optical fiber sensors have a miniaturized structure since they do not require a bulky prism. POF-SPR sensors were used for their easy manipulation, high numerical aperture (NA), and smaller bend radii. For a method of measuring RI, Bhatia *et al.* attached a 40 nm silver layer and a Si layer to the surface of an uncladding POF and tested a sucrose solution having a refractive index of 1.333 to 1.353 in steps of 0.005 [13]. Cennamo *et al.* designed a SPR sensor based on bilayer metal (Pd/Au) and a D-shaped POF, and the sensor exhibits excellent performances in the 1.38-1.42 RI range [14]. Although the structure of the POF-RI sensor is simple to process, almost half of the core is removed in those designs, which seriously degrades the mechanical robustness of the fiber.

Due to the material properties of POFs, they can be made into different structures by simple methods. The fiber is bent into a millimeter radius in order to increase the evanescent field strength [15]. Side-polished fibers [16], [17] with sandpapers have the disadvantages of high machining difficulty and inconsistent structure. Some chemicals, such as acetone, were used to corrode the fiber cladding and core [18]. The etching method will destroy the material properties of the

optical fiber and reduce the robustness of the optical fiber. Tapered fibers prepared by heat-and-pull techniques have a disadvantage of low evanescent field strength [19], [20]. In addition, as the smooth surface of fibers reduce the adhesion between optical fibers and sensitive materials, some schemes were proposed to improve the fiber structure. The twisted macro-bend coupling structure sensor is complicated and has alignment issues [21]. Multi-group groove-like structure processed by mold [22]–[24] can ensure the consistency of processing, but this processing method does not have the flexibility, and greatly increased the processing cost. In this paper, the use of a UV laser can increase the machining speed, while ensuring machining consistency and reducing machining loss. The evanescent field strength and sensor sensitivity can be increased by changing the processing parameters of the narrow groove structure.

The work described in this paper, gold layers were sputtered on the POF, with a narrow groove structure which has a great influence on the transmission power and was used to stimulate the SPR effect. The RI measurements were performed using NaCl solutions with different concentrations. The intensity interrogation is used to detect the RI, and the effects of narrow groove structural pitches on sensor's responses were studied. The experimental results show that the proposed sensor has good output response characteristics. A linear curve is used to characterize the relationship between power and RI, when the RI varies from 1.340 to 1.356. With a 400 μm machining pitch, the sensitivity of the sensor is maximized. The system's advantages include low cost and easy detection.

II. MECHANISM OF RI SENSITIVITY

RI of the test NaCl solution ranges from 1.340 to 1.356. A step-index POF (SK40, Mitsubishi, Japan) was used. The refractive index of the core and cladding are 1.49 and 1.41, respectively. One groove structure is chosen to explain the principle of the proposed sensor. An illustration of the POF-NGS (Au) sensor working principle is shown in Fig.1.

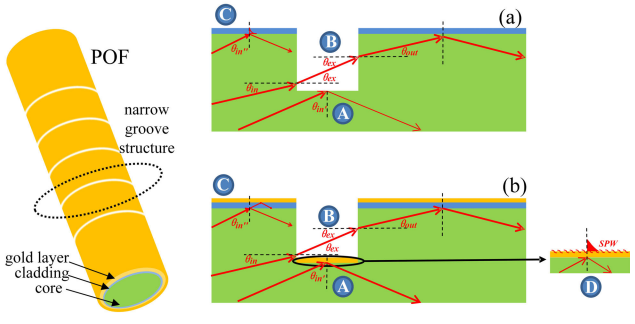

FIGURE 1. Illustration of the POF-NGS(Au) sensor working principle. (a) without gold layer (b) with gold layer.

In Fig1 (a), the transmission power in the optical-fiber without the gold film is composed of the power in the A, B and C regions. In A region, when the incident angle ($\theta_{in'}$) is greater than the critical angle (θ_c), the fiber will have total internal reflection (TIR) at the core-air interface. Where n_{air} and n_{core} are the reflective indexes of the air and core. When the external environment changes from air to NaCl solution, the critical angle at the core-air interface increases and caused the core to allow the propagation of light modes to decrease, resulting in attenuation of transmission power of the region A. In B region, when the light is transmitted to the vertical edge of the narrow groove, most of the light is lost through refraction, but part of the light will be coupled into the fiber by double refraction. θ_{in} is the angle of incidence at the narrow slot, θ_{ex} is the refraction angle of the external environment, and θ_{out} is the refraction angle of optical coupling. According to Snell's law, $\theta_{in} = \theta_{out}$, and when the refractive index of the environment (n_{ex}) increases, the refraction angle θ_{ex} will become smaller, making more light coupling into the fiber. At this time, the transmission coefficient (T) of the unpolarized light transmitted from the fiber to the external environment can be expressed as [24], [25]:

$$T = 0.5\frac{sin\,(2\theta_{in})\,sin\,(2\theta_{ex})}{sin^2\,(\theta_{in}+\theta_{ex})}\left[1+\frac{1}{cos^2\,(\theta_{in}-\theta_{ex})}\right] \quad (1)$$

where $\theta_{ex} = arcsin\,[n_{core}sin\,(\theta_{in})\,/n_{ex}]$. In C region, TIR occurs at the core-cladding and cladding-air interfaces. When the medium changes from air to NaCl solution, the critical angle at the cladding-air interface increases and caused the cladding to allow the propagation of light modes to decrease, resulting in attenuation of the light. This component of the attenuation is called Evanescent Wave (EW) loss. The above is the working principle of the fiber without gold layer.

After the gold film is sputtered to the surface of the narrow groove, the transmission power will be affected by four regions (A, B, C and D). The gold layer has a small effect on the coupling power in the B region but has a tremendous effect on the A and C region. This is because when the incident wavelength is 660 nm, the reflectance of the gold layer is close to 1 [26]. This means that when the gold layer is attached to the fiber surface, the transmission power will increase. In region D, the SPR effect causing power attenuation occur when the propagation constant of the incident light is equal to the surface plasma wave (SPW) on the surface of the gold film. Further experimental tests are performed in section III.

III. EXPERIMENTS

A. FABRICATION OF POF-NGS (Au)

A step-index POF (SK40, Mitsubishi, Japan) was used to host the narrow groove structures. The core material of the POF is polymethyl methacrylate (PMMA) with a diameter of 980 μm, and the cladding material is a fluorinated polymer with a thickness of 10 μm. The numerical aperture (N.A.) is 0.5. A UV laser (355 nm solid-state UV laser, Delphi Laser, China) was used to create the narrow groove structures on the surface of the POF. After setting the laser's frequency and duty cycle, the fiber was fixed on the laser platform for machining. Fig. 2(a) shows the schematic diagram of the

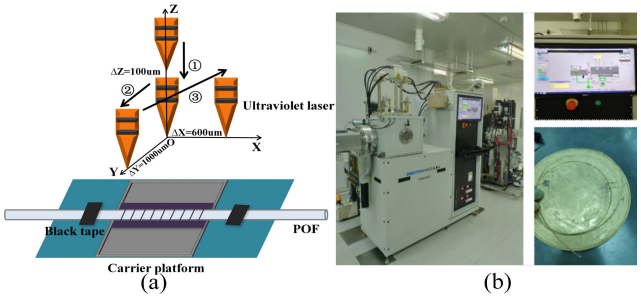

FIGURE 2. (a) Schematic diagram of laser machining. (b) Sputtering experimental apparatus and POF with gold layer.

laser machining process, as used on the fiber. The three XYZ values characterize the relative positions of the laser beam and the fiber. The X axis represents the lateral distance to the fiber, the Y axis the distance the laser moves, and the Z axis the vertical distance between the laser and the fiber. The fiber was washed with distilled water to clean its surface, and prepared for the gold layer sputtering in the next step.

The fabricated fiber was bent and fixed to a machined disk in a magnetron sputtering apparatus (NJ08057, Denton Vacuum, USA). The machining time was determined by the time needed to reach the target gold layer thickness of 100 nm. The sputtering experiment apparatus and the sputtered fiber are shown in Fig. 2(b). As shown in Fig. 2 (b), the gold layer completely covers the outer surface of the optical fiber.

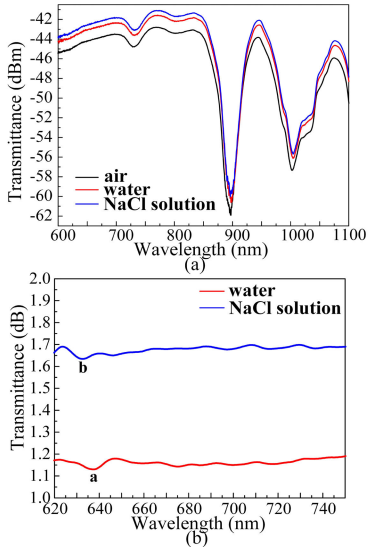

FIGURE 3. (a) The transmission spectrums of air, water and NaCl solution, (b) The transmittance spectrum of the POF-NGS (Au) sensor under water and NaCl solution.

In order to obtain the transmission spectrum of the POF-NGS (Au) sensor, we set up a wavelength-modulated experimental setup. It included a halogen lamp and a spectrum analyzer. The halogen lamp (SLS201, Thorlabs, Newston, NJ, USA) has a wavelength range from 300 nm to 2600 nm. The detection range of the spectrum analyzer (AQ6374, YOKOGAWA Test & Measurement, Tokyo, Japan) is from about 350 nm to 1750 nm. Fig. 3(a) shows the transmission spectrums of air, water and NaCl solution. The transmission spectrums of water and NaCl solution were characterized by measuring the transmission spectrum and subtracting the spectrum measured in air. As shown in Fig. 3 (b), the resonant wavelength changed from 638.2 nm (a) to 634.2 nm (b), when the RI changed from water (RI = 1.333) to the NaCl solution (RI = 1.340). The SPR effect of the proposed sensor is weak compared to other POF-SPR sensors [27]–[30]. The main reason is that the proposed structure has less damage to the core, resulting in less loss of light intensity in the test area. In addition, as the RI increases, the transmittance increases as shown in Fig 2. The change in power is more pronounced than the change in resonant wavelength, providing the basic criteria for the approach to intensity interrogation used in this paper.

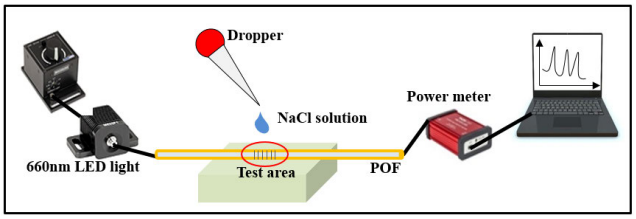

FIGURE 4. Measurements of POF-NGS (Au) sensor.

B. EXPERIMENTAL SETUP

The schematic to illustrate the experimental setup is shown in Fig. 4. The prepared POF-NGS (Au) sensor was fixed to the soft block. One end of the fiber was connected to the LED light source (M660F1, Thorlabs, Newston, NJ, USA). The LED light sources used were stable and do not require optical isolation to replace laser sources that are susceptible to echo interference. The other end was connected to the power meter (PM100USB, Thorlabs, Newston, NJ, USA), which contains a photodiode s151c. The variations in the optical output power were displayed on a computer using the optical power meter monitor software package (Thorlabs, in Newston, NJ, USA). The POF-NGS (Au) sensor (except for the test area) were put in a black cover to avoid interference from visible lights [31], as were the free ends. The RI tests were performed by dropping the NaCl solution on the test area using a dropper.

IV. RESULTS

A. CHARACTERIZATION

The micrographs of the POF-NGS and POF-NGS (Au) are shown in Fig. 5. The induced temperature rise during laser machining changes the surface strain of the fiber, and makes the edge rough. As shown in Fig. 5(b), the surface of the fiber has a metallic luster. The accumulation of edges on the structures increases the area of the gold layer on the surface of the fiber.

In order to verify the consistency of laser machining, a fiber with a period of 800 μm was selected. We characterized ten sets of values for machining width (a), machining spacing (b), and machining pitch (c), as shown in Table 1. In summary,

TABLE 1. Narrow groove parameter.

Parameters	Value of Narrow groove structure(μm)										
	No1	No2	No3	No4	No5	No6	No7	No8	No9	No10	max deviation
width(a)	57.7	56.9	56.5	57.5	56.8	57.7	56.7	56.5	57.4	57.1	1.2
spacing(b)	742.6	743.3	743.1	742.9	742.8	742.9	743.5	743.1	742.5	743.4	1
pitch (c=a+b)	800.3	800.2	799.6	800.4	799.6	800.6	800.2	799.6	799.9	800.5	0.6

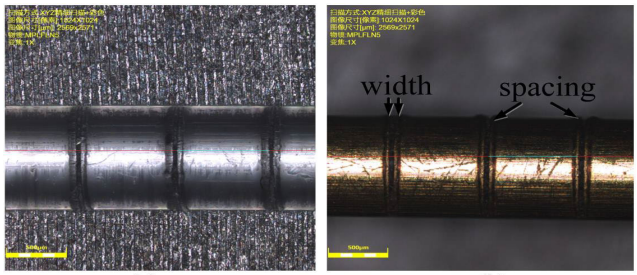

FIGURE 5. (a) Microscope photo of POF-NG. (b) Microscope photo of POF-NGS (Au).

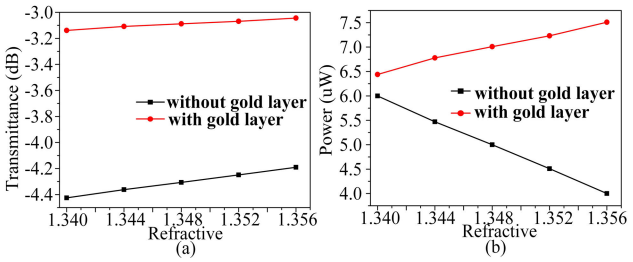

FIGURE 6. Transmission power of sensor with or without gold film in NaCl solutions (a) in dB (b) in μW.

the data in the table shows that the maximum deviation value of the machining pitch (c) is 0.6 μm. the width's deviation is small. The deviation of laser machining may come from the weak fixation of the POF. Therefore, the result shows the machining method can guarantee the consistency of the structure

B. THE EFFECTS OF GOLD LAYER ON RI DETECTION

The effect of the deposited gold layer on the RI sensor was characterized. Two POFs, 50 cm in length, were used and processed with 5 mm long narrow groove structures on their surfaces. One fiber was sputtered with a 100 nm gold layer with machining pitch 600 μm, and another fiber was not coated with a gold layer. The output responses of the two sensors to five different RI NaCl solutions were measured at room temperature (RT). The power transmittance (T) of the proposed sensor is calculated using:

$$T = 10log_{10}\left(\frac{P_{out}}{P_{in}}\right) \tag{2}$$

where P_{out} represents the output power of the NaCl solution, and P_{in} represents the initial output power without the NaCl solution at 25°C. The results are shown in Fig. 6. The SPR effect occurs due to the gold layer attached to the surface of the POF-NGS. In Fig. 6, when the POF-NGS is coated with a gold layer, the increases in transmittance and in output power are accompanied by an increased refractive index (RI). Moreover, it also can be seen from Fig. 2(b) that when the incident wavelength is 660 nm, as the RI increases the transmittance increases, resulting in increased output power. The results obtained by intensity interrogation and wavelength interrogation are consistent, indicating that the method of intensity modulation is effective and visualized. When the POF-NGS is not coated with a gold layer, the transmittance of the sensor increases with the increase of the refractive index (RI), and the change in power is opposite to the change of transmittance. The increase of the external RI reduces the difference between the core-air interface, increasing the critical angle of the two interfaces and reducing the optical transmission mode inside the POF, leading to optical fiber loss. As shown in Fig. 6(a), the slope of the transmittance curve of the POF-NGS sensor is slightly larger than that of the POF-NGS (Au) sensor. POF-NGS sensor cause the power loss under the interaction of the evanescent field, which expands the difference between the output power and the input power. According to Equation 2, it can increase the slope of the transmittance curve. In contrast, the output power of the POF-NGS (Au) sensor increases as the refractive index increases, as shown in Figure 6 (b). The difference between the output power and the input power is reduced, so the change of the transmittance will decrease. But the POF-NGS (Au) sensor can increase the signal-to-noise ratio.

C. STUCTURE MACHINING PITCH

This section is concerned with the effect of different machining pitches on the sensor response. The machining pitch was set to 400μm, 500μm, 600μm, 700μm, 800 μm, and 900μm. The output transmittance for five different NaCl solutions was tested and the insertion loss of the sensor was calculated. The insertion loss (I) of the proposed sensor is calculated using:

$$I = -10log_{10}\left(\frac{P_m}{P_0}\right) \tag{3}$$

where P_m represents the output power of the fiber after structural machining, and P_0 represents the output power without

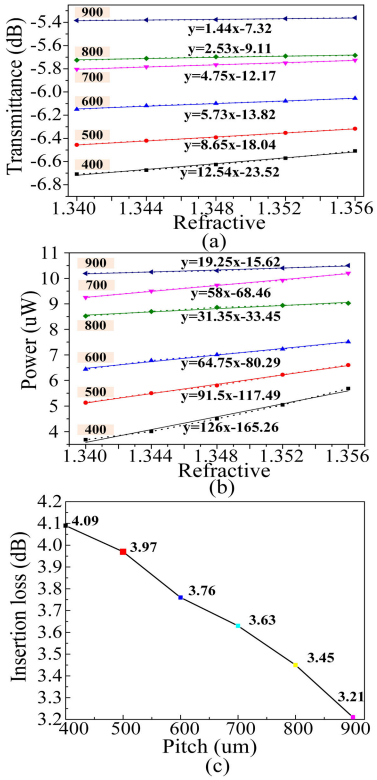

FIGURE 7. Response of POF-LPG (Au) sensor with different machining pitches, to three NaCl solutions (a) in dB (b) in μW (c) Insertion loss at different machining pitches.

any structural machining. As can be seen from Fig. 7 (a), when the machining pitch is gradually decreased, the transmittance of the POF-NGS (Au) sensor variation gradually decreases. The sensor with a machining pitch of 400 μm has the highest sensitivity, which is 12.5 dB/RIU (126 μW/RIU). By reducing the machining pitch, the sensitivity area of the surface of the optical fiber is increased, while the evanescent field increases. The sensitivity of the sensor was increased. According to the sensor principle shown in Fig. 1, it can be seen that reducing the machining pitch will increase the loss of light (corresponding to region B in Fig. 1), although the coupling power on the side will increase accordingly. As the sensitivity area between the gold film and the optical fiber increases, the power reflected by regions A and C will increase. With the increase of the machining pitch, the insertion loss is reduced, as shown in Fig. 7(c). The loss between different machining pitches is less than 0.3dB, indicating that the narrow groove structures can achieve the RI detection with small losses.

It can be seen from the experimental results that the sensitivity of the sensor is related to the narrow groove processing pitch. As can be seen from Fig. 1, the machining width also affects the coupling power, so the machining parameters (frequency and duty cycle) will become the research direction in the later period.

Fig. 7 (b) shows that the transmission power increases with the increase of the refractive index, which will increase the signal-to-noise ratio (SNR) of the sensor to a certain extent. Compared with the sensor based on evanescent wave loss, the sensor can reduce machining loss, and decrease the input power. In addition, due to the high reflection coefficient and chemical inertia of the gold film, the influence of ambient noise on the transmission power is reduced. When the sensor is placed in a normal environment, its influence on the transmission power is only a few tens of nW, which can be completely ignored compared with the output power. Therefore, the structure can increase the stability of the sensor and prolong its service life.

D. HIGH ACCURACY RI TEST

Different refractive indices ranging from 1.340 to 1.348 were prepared using NaCl in deionized water. The RI of the NaCl solution was measured using an Abbe refractometer having an accuracy of 0.0001 RIU. The POF-NGS (Au) sensor with a 600 μm pitch was used to detect the NaCl solution, and the correspondence between the refractive index (RI) and the transmittance was estimated.

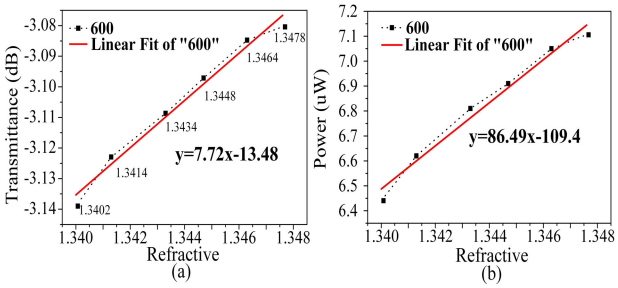

FIGURE 8. A POF-NGS (Au) sensor with 600μm pitch. (a) Output response of at RI between 1.340 to 1.348 (a) in dB (b) in μW.

The experimental results of the high accuracy are shown in Fig. 8. The relationship between the transmittance variation and the RI satisfies a linear equation, and the coefficient of determination (R^2) is 0.98. Comparing the experimental results with the results of section C, the transmission curve with a refractive index between 1.340 and 1.356 is further proved to be linear.

When the detection step size is large, the fitting curve as shown in Fig. 7(a) (b) will be obtained. Although the relation between transmission power and refractive index can be fitted as a linear relation, the output result will inevitably have deviation. Therefore, further testing is required to improve the accuracy of the output curve. As shown in Fig. 8, the experiment can further verify the linearity of the output curve.

E. REPEATABILITY TEST

The POF-NGS (Au) sensor with a 600 μm pitch was subjected to repeatability, and for test values of RI from 1.340 to 1.356 under room temperature. The experimental results are shown in Fig. 9. The multiple measurements have consistent curvature indicating that the sensor has good repeatability. There is one limitation in this structure. Gold layer losing its fastness with surface or fiber which cause after several time testing, and it reduces the corresponding output power.

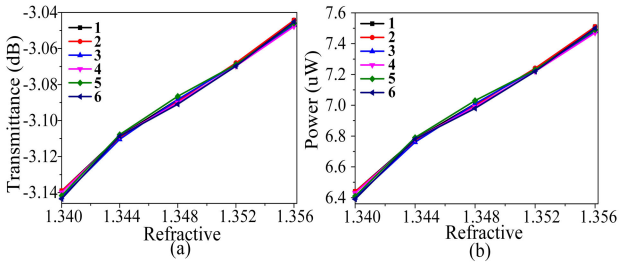

FIGURE 9. Repeatability test at RI from 1.340 to 1.356 (a) in dB (b) in μW.

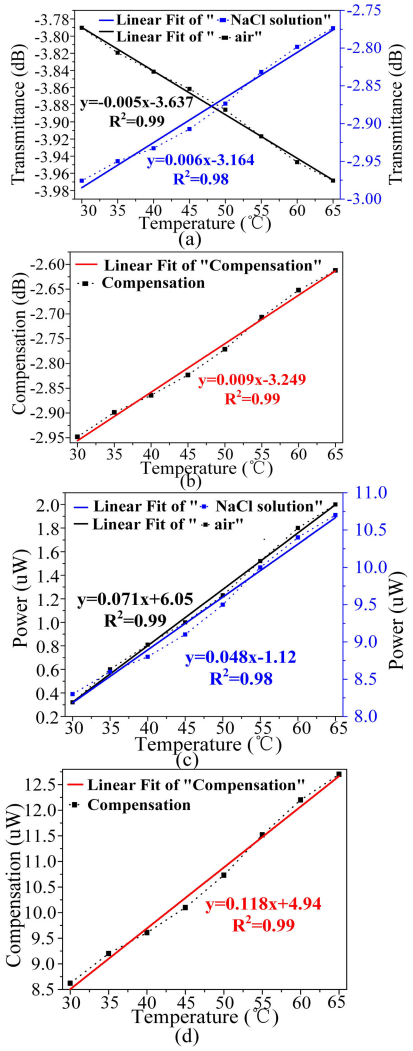

FIGURE 10. Temperature sensitivity experiment of the proposed sensor with air and with NaCl solution (RI = 1.340) (a)&(b) in dB (c)&(d) in uW.

Furthermore, this could be caused by reduced power output of the LED, as may drop with time and use.

F. TEMPERATURE SENSITIVITY EXPERIMENT

Finally, the thermo-optic (TO) coefficient of POFs is related to temperature, and temperature sensitivity property of the sensor was investigated. The POF-NGS (Au) sensor was fixed to a heating plate. A thermometer was introduced to monitor the ambient temperature of the RI sensor probe. The transmittance of the fiber at 30-65 °C was calculated, with the output power at 25 °C being the reference power. As shown in Fig. 10 (a), the transmittance of the proposed sensor is different when the temperature of the chamber is set in the range 30-65 °C. The slope of the curve changes, which means that the sensitivity of the proposed sensor is temperature-dependent. We can conclude that the change of the output power gradually declines with gradual temperature increases when the RI sensor is in the air. This is affected by thermo-optic (TO) coefficient. As the temperature rises, the refractive index of the fiber decreases, which causes the internal transmission mode and output power of the fiber to decrease. In Fig. 10 (c), when a NaCl solution is dropped on the test area, the amount of change in the output power gradually increases as the temperature rises. This is because water evaporates as the temperature rises, causing the NaCl solution concentration to increase and thereby cause the refractive index to increase too. The temperature-compensation curves were made by integrating the influence of the thermo-optic (TO) coefficient of the optical fiber and the influence of the external temperature on the sensor, as shown in Figure 10 (b) (d). It can be seen that there is a linear relationship between temperature and transmitted power. Therefore, the refractive index detection can be temperature compensated by measuring the current ambient temperature.

V. CONCLUSION

A RI sensor-based POF for monitoring NaCl solution is proposed. The proposed sensor was composed of a POF with a 50 cm length and a 5 mm narrow groove structure, and a 100 nm gold layer. Two sensing mechanisms were examined on the proposed sensor. Intensity interrogation was used for experimental detection, which greatly simplified the complexity of experimental setup and made the results intuitive. The effect of the machining pitch on the sensor's RI sensitivity was investigated. The experimental results show that there is a linear curve relationship between refractive index and output power. When the machining pitch is 400 μm, the curvature is maximized for RI from 1.340 to 1.356. The proposed sensor is easy to fabricate, and can also be integrated into systems for biological instrumentation applications, and quasi-distributed detection. The machining equipment (such as the Femtosecond laser) or method will be changed to reduce the machining width and deviations.

REFERENCES

[1] W. Qian, C. C. Chan, C.-L. Zhao, Y. Liu, T. Li, L. Hu, K. Ni, and X. Dong, "Photonic crystal fiber refractive index sensor based on a fiber Bragg grating demodulation," *Sens. Actuators B, Chem.*, vols. 166–167, pp. 761–765, May 2012.

[2] M. N. Ng, Z. Chen, and K. S. Chiang, "Temperature compensation of long-period fiber grating for refractive-index sensing with bending effect," *IEEE Photon. Technol. Lett.*, vol. 14, no. 3, pp. 361–362, Mar. 2002.

[3] F. Chiavaioli, C. Trono, and F. Baldini, "Improvement in refractive index sensitivity by means of internally curved long period fiber gratings," in *Proc. 23rd Int. Conf. Opt. Fibre Sensors*, vol. 9157, 2014, Art. no. 91578P.

[4] J. Chu, C. Shen, C. Zhong, X. Zou, K. Li, and X. Dong, "Optical fiber refractometer based on a long-period grating inscribed in a fiber loop mirror," in *Proc. Symp. Photon. Optoelectron.*, May 2012, pp. 1–4.

[5] T. Guo, H.-Y. Tam, P. A. Krug, and J. Albert, "Reflective tilted fiber Bragg grating refractometer based on strong cladding to core recoupling," *Opt. Express*, vol. 17, no. 7, pp. 5736–5742, Mar. 2009.
[6] T. Hu, Y. Zhao, and A.-N. Song, "Fiber optic SPR sensor for refractive index and temperature measurement based on MMF-FBG-MMF structure," *Sens. Actuators B, Chem.*, vol. 237, pp. 521–525, Dec. 2016.
[7] Q. Wang, L. Kong, Y. Dang, F. Xia, Y. Zhang, Y. Zhao, H. Hu, and J. Li, "High sensitivity refractive index sensor based on splicing points tapered SMF-PCF-SMF structure Mach-Zehnder mode interferometer," *Sens. Actuators B, Chem.*, vol. 225, pp. 213–220, Mar. 2016.
[8] Z. Yan, P. Saffari, K. Zhou, A. Adebay, and L. Zhang, "Optical RI sensor based on an in-fiber Bragg grating Fabry–Perot cavity embedded with a micro-channel," in *Proc. Microstructured Specialty Opt. Fibres*, vol. 8426, Jun. 2012, Art. no. 842609.
[9] B. Wang, K. Ni, P. Wang, Q. Ma, W. Tian, and L. Tan, "A CNT-coated refractive index sensor based on michelson interferometer with thin-core fiber," *Opt. Fiber Technol.*, vol. 46, pp. 302–305, Dec. 2018.
[10] M. S. Islam, C. M. B. Cordeiro, J. Sultana, R. A. Aoni, S. Feng, R. Ahmed, M. Dorraki, A. Dinovitser, B. W.-H. Ng, and D. Abbott, "A hi-bi ultra-sensitive surface plasmon resonance fiber sensor," *IEEE Access*, vol. 7, pp. 79085–79094, 2019.
[11] M. S. Islam, M. R. Islam, J. Sultana, A. Dinovitser, B. W.-H. Ng, and D. Abbott, "Exposed-core localized surface plasmon resonance biosensor," *J. Opt. Soc. Amer. B, Opt. Phys.*, vol. 36, no. 8, pp. 2306–2311, Aug. 2019.
[12] M. S. Islam, J. Sultana, R. A. Aoni, M. S. Habib, A. Dinovitser, B. W.-H. Ng, and D. Abbott, "Localized surface plasmon resonance biosensor: An improved technique for SERS response intensification," *Opt. Lett.*, vol. 44, no. 5, pp. 1134–1137, Mar. 2019.
[13] P. Bhatia and B. D. Gupta, "Surface-plasmon-resonance-based fiber-optic refractive index sensor: Sensitivity enhancement," *Appl. Opt.*, vol. 50, no. 14, pp. 2032–2036, May 2011.
[14] N. Cennamo, P. Zuppella, D. Bacco, A. J. Corso, M. G. Pelizzo, and L. Zeni, "SPR sensor platform based on a novel metal bilayer applied on D–Shaped plastic optical fibers for refractive index measurements in the range 1.38–1.42," *IEEE Sensors J.*, vol. 16, no. 12, pp. 4822–4827, Jun. 2016.
[15] C.-X. Teng, F.-D. Yu, N. Jing, and J. Zheng, "The influence of temperature to a refractive index sensor based on a macro-bending tapered plastic optical fiber," *Opt. Fiber Technol.*, vol. 31, pp. 32–35, Sep. 2016.
[16] C. Teng, F. Yu, N. Jing, Y. Ding, Z. Si, and J. Zheng, "Investigation of refractive index sensors based on side-polished plastic optical fibers," *Opt. Fiber Technol.*, vol. 36, pp. 1–5, Jul. 2017.
[17] F. De-Jun, Z. Mao-Sen, G. Liu, L. Xi-Lu, and J. Dong-Fang, "D-shaped plastic optical fiber sensor for testing refractive index," *IEEE Sensors J.*, vol. 14, no. 5, pp. 1673–1676, May 2014.
[18] D. F. Merchant, P. J. Scully, and N. F. Schmitt, "Chemical tapering of polymer optical fibre," *Sens. Actuators A, Phys.*, vol. 76, nos. 1–3, pp. 365–371, Aug. 1999.
[19] J. Shi, S. Xiao, L. Yi, and M. Bi, "A sensitivity-enhanced refractive index sensor using a single-mode thin-core fiber incorporating an abrupt taper," *Sensors*, vol. 12, no. 4, pp. 4697–4705, 2012.
[20] Y. Miao, Y. He, X. Ma, H. Zhang, B. Song, X. Yang, L. Xue, B. Liu, and J. Yao, "Low-temperature cross-sensitivity refractive index sensor based on single-mode fiber with periodically modulated taper," *IEEE Sensors J.*, vol. 16, no. 8, pp. 2442–2446, Apr. 2016.
[21] Y. Zhang, Y. Hou, W. Liu, H. Zhang, Y. Zhang, Z. Zhang, J. Guo, J. Liu, L. Zhang, and Q.-L. Tan, "A cost-effective relative humidity sensor based on side coupling induction technology," *Sensors*, vol. 17, no. 5, p. 944, 2017.
[22] J.-D. Shin and J. Park, "High-sensitivity refractive index sensors based on in-line holes in plastic optical fiber," *Microw. Opt. Technol. Lett.*, vol. 57, no. 4, pp. 918–921, Apr. 2015.
[23] P. Antunes, J. Dias, T. Paixão, E. Mesquita, H. Varum, and P. André, "Liquid level gauge based in plastic optical fiber," *Measurement*, vol. 66, pp. 238–243, Apr. 2015.
[24] C. Teng, H. Liu, H. Deng, S. Deng, H. Yang, R. Xu, M. Chen, L. Yuan, and J. Zheng, "Liquid level sensor based on a V-Groove structure plastic optical fiber," *Sensors*, vol. 18, no. 9, p. 3111, 2018.
[25] X. Lin, Y. Li, L. Ren, Y. Xu, N. Chen, H. Ju, J. Liang, Z. He, E. Qu, and B. Hu, "Low-cost multipoint liquid-level sensor with plastic optical fiber," *IEEE Photon. Technol. Lett.*, vol. 26, no. 16, pp. 1613–1616, Aug. 15, 2014.
[26] S. Babar and J. H. Weaver, "Optical constants of cu, ag, and au revisited," *Appl. Opt.*, vol. 54, no. 3, pp. 477–481, Jan. 2015.
[27] N. Cennamo, L. De Maria, G. D'Agostino, L. Zeni, and M. Pesavento, "Monitoring of low levels of furfural in power transformer oil with a sensor system based on a POF-MIP platform," *Sensors*, vol. 15, no. 4, pp. 8499–8511, 2015.
[28] C. Christopher, A. Subrahmanyam, and V. V. R. Sai, "Gold sputtered U-Bent plastic optical fiber probes as SPR- and LSPR-based compact plasmonic sensors," *Plasmonics*, vol. 13, no. 2, pp. 493–502, Apr. 2018.
[29] M. Pesavento, L. De Maria, D. Merli, S. Marchetti, L. Zeni, and N. Cennamo, "Towards the development of cascaded surface plasmon resonance POF sensors exploiting gold films and synthetic recognition elements for detection of contaminants in transformer oil," *Sens. Bio-Sensing Res.*, vol. 13, pp. 128–135, Apr. 2017.
[30] N. Jing, J. Zhou, K. Li, Z. Wang, J. Zheng, and P. Xue, "Refractive index sensing based on a side-polished macrobend plastic optical fiber combining surface plasmon resonance and macrobending loss," *IEEE Sensors J.*, vol. 19, no. 14, pp. 5665–5669, Jul. 2019.
[31] A. Ghaffar, Y.-L. Hou, W.-Y. Liu, F. A. Dharejo, H.-X. Zhang, P. Jia, H. Yanyun, J. Liu, Z. Yunjun, and Z. Nasir, "Two-dimensional displacement optical fiber sensor based on macro-bending effect," *Opt. Laser Technol.*, vol. 120, Dec. 2019, Art. no. 105688.

YANJUN HU was born in Heilongjiang, China, in 1991. She received the B.S. degree from the School of Instruments and Electronics, North University of China, in 2015, where she is currently pursuing the Ph.D. degree. Her current research interests include the study of optical fiber sensors for humidity, gas, and distributed measurements.

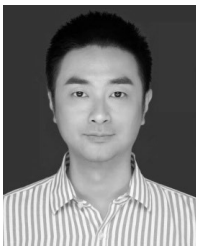

YULONG HOU was born in Shanxi, China, in 1984. He received the Ph.D. degree from the School of Instruments and Electronics, North University of China, in 2015. He is currently a Lecturer with the North University of China. His current research interests include the study of optical fiber sensors for liquid level and liquid leakage measurements.

ABDUL GHAFFAR was born in Pakistan, in 1991. He is currently pursuing the Ph.D. degree in instrumentation and measurement technology with the North University of China. Previously, he was a Lecturer with Indus University Karachi, Pakistan. His research directions are sensors technology, optical fiber sensor, distributed sensor, and displacement sensor.

WENYI LIU was born in Shanxi, China, in 1970. He is currently a Full Professor with the Institute of Instrumentation and Electronics, North University of China. He is also mainly involved in teaching and researching in the field of measurement technology and instruments. His current research interests include distributed data recording systems, wireless sensor networks, embedded systems, lossless compression coding, data encryption, multifunctional structure, wireless sensor networks, special optical sensors, and new high-speed data transmission bus development work.